Advances in Multi-Scale Characterization Techniques of Bone and Biomaterials Interfaces

Dakota M. Binkley[1], Kathryn Grandfield[1,2]

[1]Department of Materials Science and Engineering, McMaster University, Ontario, Canada

[2]School of Biomedical Engineering, McMaster University, Ontario, Canada

* Corresponding author: kgrandfield@mcmaster.ca

ABSTRACT

The success of osseointegrated biomaterials often depends on the functional interface between the implant and mineralized bone tissue. Several parallels between natural and synthetic interfaces exist on various length scales from the micro-scale towards the cellular and the atomic scale structure. Interest lies in the development of more sophisticated methods to probe these hierarchical levels in tissues at both biomaterials interfaces and natural tissue interphases. This review will highlight new and emerging perspectives towards understanding mineralized tissues, particularly bone tissue, and interfaces between bone and engineered biomaterials at multi-length scales and with multi-dimensionality. Emphasis will be placed on highlighting novel and correlative X-ray, ion, and electron beam imaging approaches, such as electron tomography, atom probe tomography, and *in situ* microscopies, as well as spectroscopic and mechanical characterizations. These less conventional approaches to imaging biomaterials are contributing to the evolution of the understanding of the structure and organization in bone and bone integrating materials.

1. INTRODUCTION

Continued advances in biomaterials development and characterization stem from the need for biomedical devices to facilitate the functional repair of tissues. One such tissue that biomaterials technologies are still sought to repair is bone tissue. Specific interest lies in bone augmentation or regeneration, joint replacement, and dental restoration technologies, where maintenance of bone health and quality in these scenarios is integral to restoring daily functions such as, skeletal mobility, and mastication.[1] Bone, however, is a hierarchical material with heterogeneous structure and chemistry across multiple length scales.[2] This complexity has made the development and understanding of the attachment of bone to implant materials, or osseointegration, an ongoing challenge.[3]

Therefore, to further the investigation of biomaterials towards osteogenic applications, we require a complete understanding of the mechanisms at the bone-interface, and also the natural interphases within the host bone tissue. An interface can be described as the abrupt connection between two differing materials, for example with distinct differences in chemical or mechanical properties, such as bone and titanium. Quite similar to an interface, the term interphase has been used to describe the location where two materials conjoin, however, this junction is comprised of a gradual change between two materials composed of comparable chemical constituents or materials properties, a prime natural example of this are the interphases within teeth: the cementum-dentin-junction and the dentin-enamel- junction. [4] Our group has contributed toward this field by the development of multi-dimensional and multi-length scale characterizations of osseointegrated materials interfacing to bone tissue.[3,5,6]

In this review, we aim to provide insights into a wider array of novel approaches to investigate bone, its natural interphases, and the bone-implant interface. After a brief introduction on bone and osseointegrated implants, the review is organized by the length scale from the micron and cellular level, to the nano and atomic scale, to real-time processes for the investigation of mineralization. Special emphasis is placed on electron, X-ray and ion-based imaging techniques that can be used to resolve bone structure and bone-implant interfaces along their many hierarchical levels, however spectroscopic and mechanical characterizations are also briefly mentioned. This work aims to highlight less conventional techniques that are making their mark on the landscape of osseointegration and biomineralization research. The structure of the review, and breakdown of techniques covered, is further outlined in this brief table of contents:

2. THE MINERALIZED INTERFACES OF INTEREST

Bone: Structure and Organization

Prior to understanding how biomaterials integrate with bone tissue, it is important to grasp the basics of the structural and chemical organization of bone. Bone is comprised of two main components: collagen, an ubiquitous protein found in many tissues, and bone mineral, specifically a calcium phosphate in the form of either hydroxyapatite (HA), carbonated-HA (cHA), or amorphous calcium phosphate (ACP).[7] By weight, bone consists of roughly 65% mineral and 35% collagen. This composite structure is responsible for the optimal materials properties displayed by bone, specifically, its inherent strength and toughness.[8,9] These core components of collagen and hydroxyapatite form the mineralized collagen fibrils that create the building blocks of higher order architectures that are intricately organized on multiple length scales, such as collagen fibers and osteonal lamellae.[8,10] Some of these hierarchical features are outlined in **Figure 1**. At even higher-level architectures bone can be separated into two forms, trabecular (cancellous) spongy bone and cortical or compact bone. This hierarchical structure further provides bone with increased durability, making the skeleton less susceptible to skeletal fractures upon mild impacts.[9] In addition to mechanical integrity, bone hosts many biological functions such as storing bone marrow, which contains the adaptive immune response and governs blood cell production.[11] Furthermore, bone is a dynamic material, constantly remodeling

throughout its lifetime to adapt to mechanical loads, and chemical signals.[12,13] More recent works

that review bone hierarchical structure are widely available.[14]
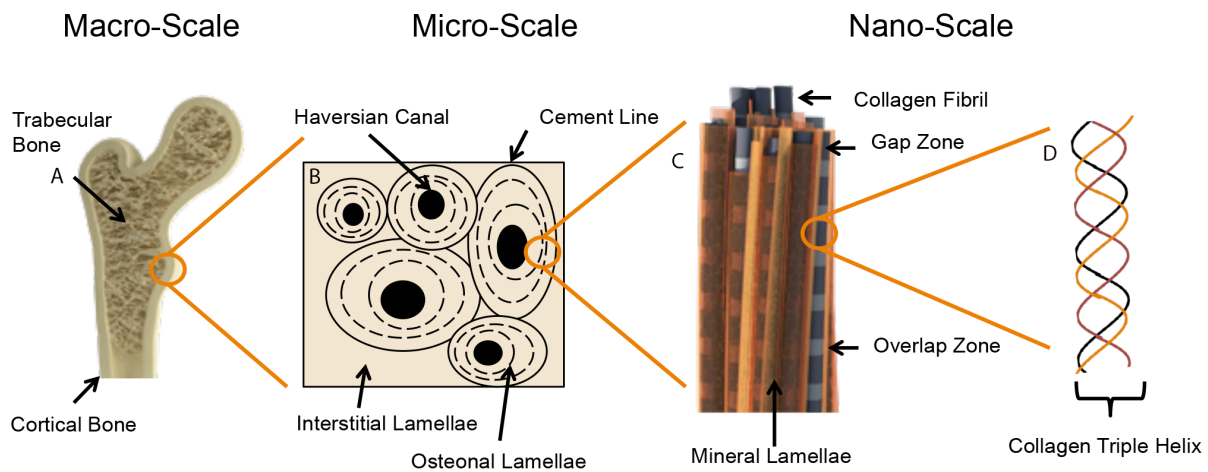
Figure 1. Hierarchical structure of bone from the macro to nanoscale. (A) At the macro-scale, bone is organized into the well-known structures of cortical or trabecular bone. Moving to successively smaller length scales, (B) osteons and trabeculae (not shown) comprise the basic micro-scale structural units of bone. Cortical bone is organized such that multiple Haversian canals run through each set of concentric osteonal lamellae. The cement line is a highly-mineralized component of the osteon, which is the interphase between the osteon and the interstitial lamellae. (C) On the nanoscale, bone is comprised of mineralized collagen fibrils, where a predominant amount of bone mineral surrounds the apparent collagen banding pattern of gap and overlap zones (adapted with permission from [141]), (D) formed by the staggered connection of Type I collagen molecules with their characteristic triple helix structure.

Biomaterials for Osseointegration

Brånemark was the first to coin the term osseointegration as the functional connection between

bone and implant devices in the 1950s.[15] Since then, biomaterials have been investigated for their

potential to osseointegrate with bone. This connection is governed not by surgical

methodologies, but by the ability of bone-forming cells, osteoblasts, to secrete mineral towards

and on foreign objects, integrating them within the native bone to create an attachment to the

implant surface that supports mechanical loading.

Several materials are used in osseointegrated implants, but titanium has garnered the most

attention as an implantable material for correcting bone fracture, joint replacement, and tooth loss.[16,17] The success of this material relies on its biocompatibility, which has been attributed to the inherent oxide layer on the metal surface.[18] In addition, the suitable mechanical properties of titanium provide the necessary strength to allow the skeleton to maintain its structural integrity[17]. Of course a plethora of other natural and synthetic bone implant materials are regularly used, sometimes in conjunction with titanium implants, including bone grafts: either autografts, bone material from the host, or allografts from a donor[19,20]. These grafts, and other natural biomaterials such as proteins[21] and polymer matrices[22] can either be directly placed in wound sites or around titanium bone implants, in hopes of increasing bone growth and ultimately minimizing device failure.[20]

Despite the potential titanium shows as an appropriate bone integrating biomaterial, complications arise due to the increased elastic modulus titanium has in comparison to bone. As titanium is much stiffer than bone, it can over compensate for surrounding bone tissue, resulting in the resorption of host tissue; a process termed stress-shielding, further reviewed elsewhere.[23] However, it is believed that the formation of a gradual interphase and strong integration between bone and implant would allow transfer of loading and effectively decrease the effect of stress-shielding.

Similar to the tissue with which it bonds, the bone-implant interface is hierarchical in structure, **Figure 1**. Despite great advances in titanium bone-implant design and surgical implantation practices, failure rates among these materials remain sufficiently high, with implant loosening or osteolysis contributing to a large portion of failures[3], and increased patient risk for secondary

6

surgeries.[24] While biomaterials are being engineered daily to solve these problems of integration, assessment of these with suitable techniques is constantly developing with technological advances in software, hardware, and data handling methods. Approaches to some less conventional techniques to enable visualization of this bone-implant interface across hierarchical levels are presented here, with some examples outlined initially in **Figure 2**.
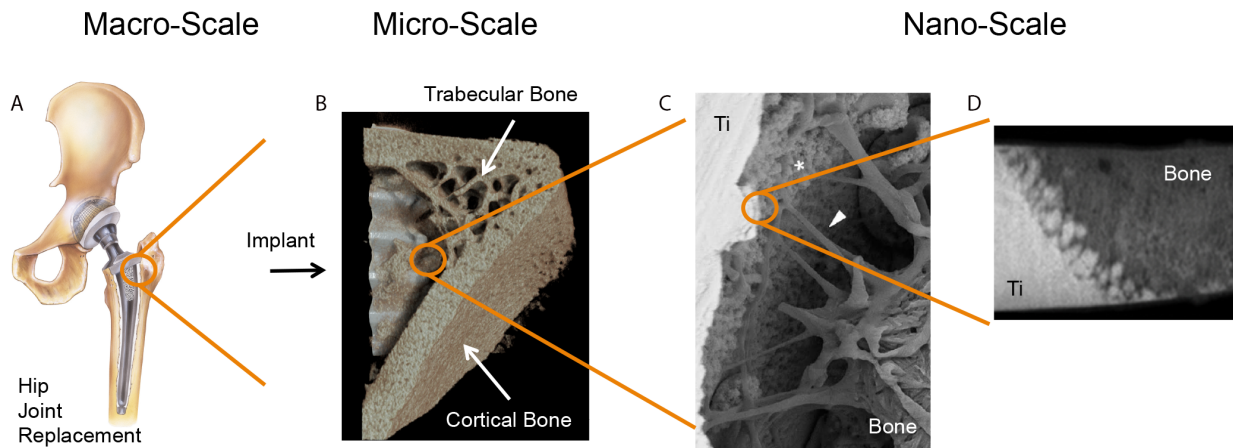
Figure 2. Hierarchical characterization of osseointegration from the macro to nanoscale. Similar to bone, the connection at bone-implant interfaces spans several length scales. As an example, (A) a titanium hip joint or dental implant in connection with bone can be visualized by (B) micro-computed tomography, demonstrating the overall bone growth towards the implant material, as well as trabecular and cortical micro-scale structure. (C) Using SEM, the importance of cellular attachment to the implant material is clear, and (D) once further magnified by TEM, a clear nanoscale integration is visualized, where the bone and implant material seem to mix with one another. Adapted with permission from our works in [6,34,49].

3. AT THE MICRON AND CELLULAR LEVEL

Electrons, X-rays and ions:

Historically, interphases in bone tissue and bone-implant interfaces were investigated using traditional life-science microscopical approaches, such as light microscopy, and more specifically histology. These methods were used to evaluate bone health through the identification of relevant biological cells, such as osteoblasts and osteoclasts[25,26]. However, while biologically relevant, these approaches are limited by the resolution of the light microscope. The use of X-rays, electrons and ions as imaging sources has enabled an increase in resolving power and allowed more advanced imaging techniques that could be used in both clinical and research settings. Herein, we will discuss novel imaging approaches for understanding features of bone structure and biomineralization that have emerged at the micron scale and level of cellular structures in bone.

The micron scale, where bone units are represented by osteons and trabeculae, is of interest for the evaluation of both bone pathology and osseointegration. At this essential level, the most basic characterization approaches include scanning electron microscopy (SEM), and microcomputed tomography (micro-CT), with focused ion beam (FIB) microscopy bringing the newest perspectives to the field. A complete summary of all of the techniques presented at each length scale can be found in **Table 1**.

Table 1. A brief list of imaging and spectroscopic techniques used to assess bone tissue and bone-implant interfaces and their respective benefits and limitations.

Technique	Benefits	Limitations	References
At the Micron and Cellular Level			
SEM	Compositional information Surface topology Can be coupled with e.g. AFM and FIB Good depth of field	2D imaging Potential electron damage Bone must be dehydrated Sample coating with a conductive layer is usually required	27-29, 38, 40, 49, 50, 56 – 58, 107, 109
Micro-CT	3D visualization at micron scale Dry and wet conditions	X-ray attenuation artifacts if material density differs e.g. bone and metal Limited resolution to several microns (unless using synchrotron source)	30, 33, 35, 50
FIB Tomography	3D visualization Nanoscale resolution	Destructive technique Potential for ion beam damage to biological materials	10, 37, 38, 42, 44
At the Nanometer Level			
SAXS	Ability to determine structural information, mineral crystal size, orientation and thickness	Low signal to noise ratio Intensive post-processing of data Synchrotron source required	53, 54
TEM	Multiple imaging modes (e.g. BF, DF, HAADF, STEM) Couple with characterization tools (e.g. EDS, EELS) Nanometer resolution	Intensive sample preparation Small sample size Potential for electron beam damage Samples must be dehydrated	11,19–36
Electron Tomography	3D visualization of mineral and collagen interplay High-resolution	Physical limitations based on rectangular sample geometry (missing wedge) Potential for electron beam damage due to long acquisition times Intensive post-processing of data Sample must be dehydrated	18, 37, 39, 48, 55, 59, 60, 62-64, 66-70, 86, 111, 117, 115
Liquid Cell	Real-time observation of mineralization Samples maintain hydrated state (natural environment)	Decreased image resolution due to electron scattering events in liquid Beam induced mineralization Confined liquid volume	61, 106, 116, 118, 119, 121-124, 126, 128
At the Atomic Level			
APT	3D imaging and chemical information High spatial resolution High chemical sensitivity	Data collection limited by sample fragility, low conductivity, heterogamous crystal and organic structure Intensive sample preparation Complex reconstruction and data processing	86-96

SEM uses a focused electron beam rastered across the surface of a specimen to produce several signals for imaging and elemental analysis. Secondary electrons which are generated within the sample are collected to form images with topological features, while backscattered electrons (BSE) that originate from the electron column and are rebounded from the first few layers of the specimen provide compositional contrast that provides insight into variations in bone structure and mineral content, where highly mineralized areas appear brighter. The composition can be further characterized by energy dispersive X-ray spectroscopy (EDS), whereby the interaction of the electron beam within the sample releases characteristic X-rays that are detected and can be quantified.

A critical SEM based technique, quantitative backscattered electron (q-BSE) imaging has become a hallmark for evaluating bone structure and bone-implant contact on the micron level, providing chemical information that can aid in robust estimates of bone quality. q-BSE relies on interactions of the primary electron beam with the sample. The quantity of BSE that escape the sample, and therefore the signal intensity, increases upon interaction of the primary electron beam with higher atomic number (Z) elements, resulting in images capturing Z-contrast.[27] If the SEM is calibrated to standards, the intensity of the peaks can be related to the concentration of each element that interacts with the beam.[27] More recently, the technique continues to prove valuable in the assessment of pathological conditions in bone, including investigations of osteoporosis[28], and rheumatoid disorders.[29] While SEM has several advantages including relatively high resolution (~1nm), compositional contrast, and ability for elemental analysis, it is limited in dimensionality, that is, it is a 2D imaging approach.

Microcomputed tomography (micro-CT) is a non-destructive method of three-dimensional (3D) imaging that can be used to evaluate the overall bone growth around biomaterials, or bone itself. With slightly lower resolution than SEM, micro-CT offers the primary advantage of 3D imaging. The sample is generally rotated around 360° or 180° and X-ray micrographs are recorded at each angle, such that mathematical algorithms can be applied to these images to produce an accurate 3D representation of the sample volume. Micro-CT is made possible by the attenuation of the X-rays changing as it passes through the sample, with beam intensity decreasing depending on the composition of the sample through which it interacts.[30] Advanced data processing and visualization pipelines allow for specific volume rendering and segmentation, which ultimately aids in the quantification of the materials of interest, for example, surface area and pore volume measurements. In addition to imaging, X-ray based approaches that probe structural or chemical information can be combined with tomography at synchrotron sources which are well equipped for multiple experiments, such as small angle X-ray scattering (SAXS), and X-ray fluorescence (XRF). However, it is important to note that these analyses may produce large datasets, which present challenges for storage and processing. These techniques will not be discussed here in detail, but other articles provide an introduction to the techniques and their applications in bone and biomaterials.[31,32] In the context of biomaterials, the features typically investigated by micro-CT are usually macro-scale porosity[33], quantification of bone growth around and into *ex vivo* implants, or calculations of metrics to evaluate osseointegration, such as either the percent bone area or bone-implant contact. [34,35] Structural X-ray techniques are usually reserved for evaluating the mineral components of bone, such as orientation of osteons and collagen fibrils.[36]

Focused ion beam (FIB) tomography, sometimes referred to as FIB-SEM tomography, is a high-resolution destructive 3D imaging technique used to evaluate materials with the resolving power similar to SEM. A FIB microscope is a dual-beam microscope that combines the electron column of a SEM, with an ionized beam, such as gallium or xenon, that can be used for several functions, including the site-specific milling and deposition of material inside the microscope. FIB tomography relies on the use of a line-of-site process in which a sample is cut using a stream of ionized atoms, which act similar to a nano-scale sandblaster, to precisely mill away a block face. The milled surface is then sequentially imaged using the electron beam to create a number of serial images throughout the volume of the specimen, which are then reconstructed into the 3D volume of the material.[37]

Although used extensively in the microelectronics industry, the use of FIB in the biological domain is finally gaining acceptance, in part due to demonstration of the technique to limit beam-induced damage[38], and several comprehensive reports which highlight its use in biological imaging.[39,40] The technique has been used in both biomineralization and biomaterials research, for example to probe the bone ingrowth into commercial dental implants[41], and to track the osteocyte network in bone (featured in more detail in the following section).[42]

More recently, FIB tomography has received renewed interest for uncovering some of the microstructural features of lamellar bone. For example, Reznikov et al. have used the approach widely to investigate the 3D volume of lamellar rat bone[43], and human bone[10,44] in great detail. These studies, that encompass datasets of several microns cubed, with nanometer resolution, set the bar for FIB investigations of minerals and biomaterials by FIB tomography. It is important to

note however that this work has been performed on demineralized specimens. Real interest exists in moving towards investigating less-manipulated bone models, i.e. materials that have not undergone chemical altering methods such as preservation, demineralization, dehydration, or freeze-thaw cycles that may damage architectures.

Visualizing the osteocyte network: A Complimentary Approach

As with any intricate material, imaging hierarchical details cannot be achieved by a sole technique, thus requiring a complimentary set of characterization approaches to be applied. When characterizing bone, the cellular components on the micron scale are clearly also of interest, in particular the osteocytes of bone which are responsible for maintaining its dynamic turn over process, bone quality, strength and integrity.[45] Once osteoblasts fulfill their role in laying down new bone matrix, they become embedded in the tissue and terminally differentiate into osteocytes[46]. Osteocytes are responsible for the mechanotransduction and signaling in bone to initiate remodeling in the case of micro-fractures and other defects in bone structure.[1,45,46] The orientation of apatite mineral in bone, which contributes to its overall strength and resilience, is also dependent on the orientation of osteocyte lacunae.[47] Therefore, osteocytes have been studied widely, and are good candidates to exemplify multiple micron-scale characterization approaches.

Osteocytes have also been postulated to play a significant role in osseointegration, as direct connections between osteocytes and implant surfaces have been documented both by transmission electron microscopy (TEM) and a novel resin cast etching SEM approach.[48–50] For instance, a lack of osteocyte maturity within porous titanium implants relative to native bone was reported by Shah et al. using novel resin cast etching SEM, which suggests that nearing porous

implant features bone is remodeling differently (**Figure 3A**).[50] Ultimately, clear visualization of these networks is integral to understanding bone remodeling at biomaterials surfaces.

The osteocyte network or lacuna-canalicular network (LCN) includes the sites which osteocytes occupy, lacunae, and their connections throughout bone, canaliculi. The LCN is a unique feature of bone that illustrates how a variety of micro-scale analyses that we discussed above can be employed to investigate its architecture, some of which are highlighted in **Figure 3**.
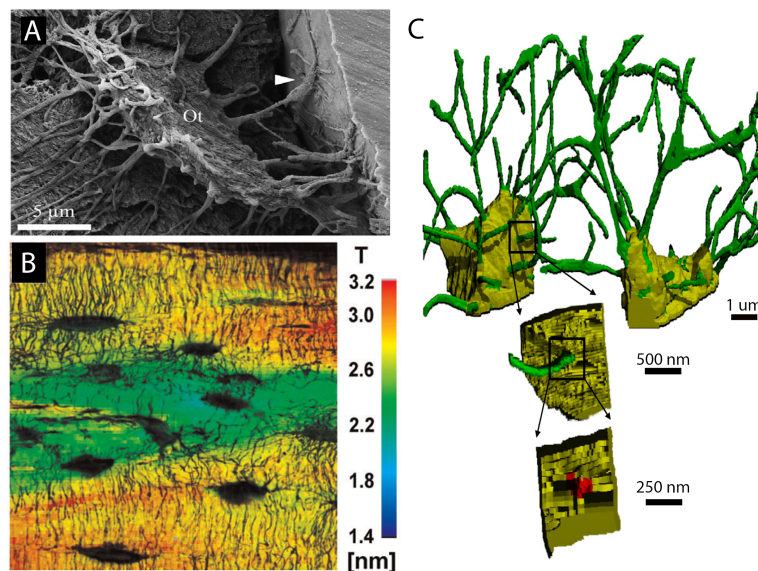
Figure 3. The osteocyte at the micro-scale. Various approaches are applied to visualize the lacuna-canalicular network (LCN). (A) A novel resin cast etching technique and SEM imaging of an isolated osteocyte (OT) with arrow pointing to canalicular attachment directly to an implant surface, suggests osteocytes contribute to successful osseointegration. (B) SAXS measurements of bone mineral particle thickness (T-parameter maps) overlaid on the osteocyte network demonstrate the variation in mineral thickness around osteocytes. (C) Using FIB tomography, a 3D rendering of the LCN highlights the spatial relationship between the osteocyte lacunae (yellow) and canaliculi (green) in a mouse femur. Reproduced with permissions from[42,50,51].

Prior to work presented by Schneider et al., **Figure 3C,** the LCN had never been characterized in 3D, arguably due to a lack of sophisticated sample preparation methods for high-resolution tomography such as FIB-SEM serial sectioning.[42] In this work, Schneider et al. imaged the LCN

in 3D using FIB-SEM tomography, and after formidable data reconstructions final renderings yielded resolution in the order 30 nm providing authors with reconstructions that could aid in determining LCN morphometry, clearly identifying the connectivity between the osteocyte lacuna and the canaliculi. [42]

Pacureanu et al., have further demonstrated the value of imaging the LCN in 3D through work applying synchrotron radiation tomography, where a monochromatic X-ray beam is passed through the sample with much higher photonic flux than traditional micro-CT. [51] Resulting images have high levels of noise, making it challenging to image cell dendrites and therefore gain information regarding bone quality.[51] These authors have shown proof of concept that their tomography data has the ability to increase the signal to noise ratio of the LCN, and successfully image cell dendrites. An overview of relevant approaches to characterize the LCN by 3D methods is well reviewed elsewhere.[52]

Moreover, additional synchrotron source X-ray analyses, such as microtomography and small angle X-ray scattering (SAXS) present many advantages for the analysis of bone mineral, particularly the LCN by simultaneously providing images or 3D structure with elemental or crystallographic information, as seen in **Figure 3B**. Similarly to SEM, during SAXS acquisition of mineralized tissues, a focused X-ray beam is rastered over the material, but instead of collecting electron information, diffraction patterns are detected. Throughout this process the tissue is rotated by various angles, such that the entire sample can be analyzed.[53]

Studies with SAXS, such as one completed by Kerschnitzki et al., have shown that mineral platelets align perpendicular to osteocytes, and that mineral particle thickness varies in the vicinity of osteocytes, after intense post-processing of the data is completed.[54] The authors demonstrated how bone architecture is related to bone quality, and successfully showed that more organized bone has smaller mineral particles nearing the osteocyte network (**Figure 3**B), meanwhile, less organized bone has larger more disorganized particles nearing these features, not shown.[54] This work is further evidence of the importance of osteocyte networks in governing bone quality, and the use of correlative imaging methods to assess these cellular features in 3D.

4. AT THE NANO AND ATOMIC SCALE

Transmission electron microscopy:

The mineralization and osseointegration landscape has been dominated by observations with light-based methods such as histology and histomorphometry, and lower resolution SEM imaging. However, to move towards an understanding of collagen-mineral interactions we need to move towards nanoscale and atomic characterizations, where TEM plays a key role. A plethora of observations that have laid foundations for understanding osseointegration of various biomaterials have been made using TEM in the 1990s.[55–58] The premise of TEM imaging relies on electrons passing through an electron transparent specimen. Once the beam is transmitted, both inelastic and elastic scattering events can be detected, and used for imaging and elemental analysis. Traditional methods of TEM imaging include bright field (BF) and dark field (DF) imaging, relying on the collection of transmitted, and diffracted electrons, respectively. More recently, the use of scanning TEM (STEM) and high angle annular dark-field (HAADF)

detectors has enabled better compositional contrast in bone imaging.[59] In this imaging mode, image intensity is roughly proportional to Z^2 (atomic number squared). This enables differentiation between mineral and organic components, and sufficient contrast of collagen fibrils without staining. The presence of nano-crystallinity in bone means that DF images can be used to identify mineral platelet orientation, and selected area electron diffraction patterns can also be used to gain information of texture. An added benefit of TEM is also its coupled spectral analyses: energy dispersive X-ray spectroscopy (EDS) and electron energy loss spectroscopy (EELS) which detect characteristic X-rays or measure characteristic energy losses to determine chemical composition. An important consideration when moving towards higher resolution analyses, such as TEM, is the sample preparation of tissues and specimens. Historically, specimens have been prepared by slicing thin sections with a diamond blade, a process called ultramicrotomy.

The advantages of using another technique, called focused ion beam (FIB), as a method to maintain interfacial integrity between bone components, and at bone-implant interfaces or in biological systems has been clearly demonstrated in recent years.[39,40]. The site-specific approach allows for isolation of a region of interest several microns wide for bombardment with gallium ions, extraction by an *in situ* micromanipulator or ex-situ method, and placement on a TEM grid for further work. These specimens are typically a maximum of 300 nm thick, allowing for electron transparency with minimal physical damage to the sample. The benefits of using this approach as compared to ultramicrotomy are widely demonstrated in ivory[60], fluorapatite-gelatine composites[61], tooth [62] biomaterial-cell interfaces[63,64], and bone-implant interfaces[65]. Schwarcz et al. have used ion milling to suggest their new model for the

ultrastructure of bone, highlighting the importance that subsequent studies to support or refute this ultrastructure should be done using similar sample preparation methods.[66] FIB techniques are also advantageous for both organic and soft tissues, as the precise milling technique minimizes damage to soft tissues[39], and can also be considered for cryogenic TEM lamellar preparation as shown for microorganisms[67], as the interest in maintaining the native state of biological tissues remains a challenge during conventional TEM.

Utilizing ion milling or focused ion beam milling new observations supporting an increase an abundance of extrafibrillar mineral in bone have been made by Schwarcz and colleagues with TEM.[66,68] Their model of bone is presented in our hierarchical view of bone in **Figure 1**. Other studies have also suggested, although to a lesser extent, the presence of higher amounts of extrafibrillar mineral[69] than originally suggested by the first ultrastructural models of bone that place most of bone mineral within the gap zone of collagen fibrils.[70,71] Biomechanical simulations of bone strength, stiffness, and finite element modeling experiments [72], have also indicated a higher likelihood that the majority of mineral is located exterior to the collagen fibrils, as in Schwarcz et al.'s model.[73]

Electron tomography:

While many imaging techniques can be used to evaluate the bone-implant interface, an optimal approach may be using correlative imaging platforms to provide a holistic view of the mineralized tissue or bone-implant interface. Such advanced platforms include the use of multi-length scale and multi-dimensional imaging techniques that can describe bone-implant contact on the multiple hierarchical levels that relate to bone structure. [3]

The use of TEM to resolve collagen-mineral interactions has been highlighted above, yet this yields two-dimensional images of distinctly three-dimensional objects. Electron tomography allows the visualization of samples in three-dimensions, providing insight to the orientation and connectivity at biointerfaces. This involves taking multiple projection images at various tilt angles, followed by the alignment and reconstruction of the images to yield a 3D volume. The basics of electron tomography are covered in detail elsewhere[74,75], including comprehensive reviews on electron tomography for applications in soft materials and biomaterials.[76,77] In general, electron tomography uses an approach that is quite similar to that employed in micro-CT. In both cases, projection images that are a monotonic function of the sample are acquired around the specimen, and then reconstructions are performed using mathematical algorithms. The resulting information is a 3D volume that can be sliced through in the Z-direction or visualized in 3D. Besides of course the obvious difference in source (electrons versus X-rays), the main difference between the two techniques is final resolution, which is dependent on the source. Electron tomograms can be obtained down to even atomic-scale resolution[78], whereas the resolution of X-ray tomography depends on the source, with synchrotron sources approaching a few nanometers, and lab-bench versions hovering around the micro-scale.

While electron tomography has had foundations in bone ultrastructural observations, the first pioneering works in this area utilized either bright-field or high voltage tomography.[79–81] Newer approaches to electron tomography, specifically a form that uses high-angle annular dark-field (HAADF) images to gain compositional contrast, have been demonstrated to support claims of

new ultrastructural models of bone[82], understand the orientation of bone adjacent to osteocyte lacunae[49], and to understand the orientation of collagen fibrils and interfacial connections at biomaterial interfaces, such as hydroxyapatite-bone[65], titanium-bone[18,34,83], and dental cement-dentin interfaces[84].

New developments in electron tomography are related to increasing the accuracy of reconstructions to allow more quantitative understanding of interfaces, for example, by reducing artifacts from the missing-wedge by moving to a 180° rotation tomography, called on-axis electron tomography. This approach was demonstrated by us to show clear morphological features of nano-roughened titanium oxide integrating with human bone.[6] Other emerging directions include simultaneous electron tomography and elemental analyses to offer information on chemical signals. One such approach is EDS tomography, the developments of which and remaining challenges are highlighted for nanoparticle systems.[85] This technique collects EDS maps at each imaging step during tomography acquisition, which can then be reconstructed similarly to images to gain a 3D compositional map. A similar approach using electron energy loss spectroscopy (EELS) tomography been demonstrated on bone-implant interfaces, where the chemical signatures assist in the differentiation of collagen and mineral phases[86], where EELS detects the energy lost from inelastically scattered electrons that are characteristic to each element.
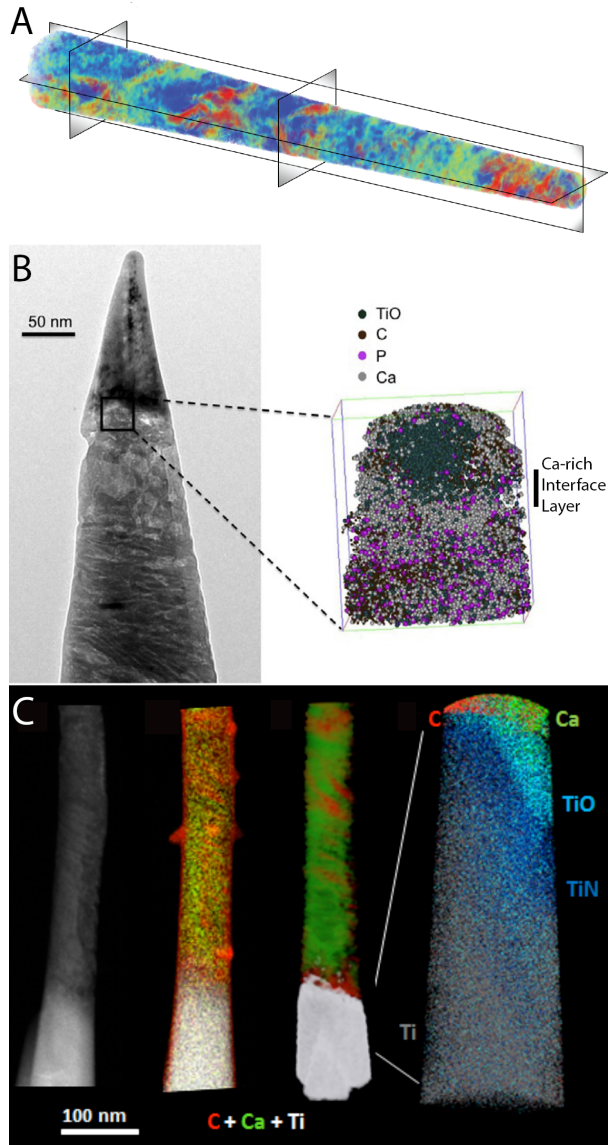
Atom probe tomography:

Shifting to yet smaller length scales, atom probe tomography (APT) offers extensive capabilities for high resolution imaging at the atomic scale with a spatial resolution of sub-0.3 nm, while

simultaneously revealing chemical information achieving a sensitivity of 1 ppm.[87] The fundamentals of APT rely on successive field evaporation of atoms as ions from the specimen surface by an applied high voltage field or a pulsating laser. The use of electric field is primarily employed for samples of high electrical conductivity; meanwhile, the pulsating laser enables field evaporation of non-conductive materials. The evaporated ions are detected laterally (x,y) by a position-sensitive detector, and due to the nature of the pulsating laser, the exact atom evaporation and time-of-flight can be detected for each atom. The combination of these parameters yields the exact z-coordinate of each atom and respective mass-to-charge (m/z) ratio.[87]

While a technique initially thought to be reserved for conductive and non-biological samples, a plethora of applications for APT are arising in biology and biological materials. For example, chemical mapping of mammalian HeLa cells by APT has been demonstrated[88], as well three-dimensional reconstructions of ferritin[89], chiton[90], and a host of other biominerals including various apatites[91], and enamel[92–94].

Recently, we presented the first APT of human bone, which highlights the distribution of trace elements, such as sodium, within the organic regions of bone, and at organic-inorganic interfaces, not otherwise detectable with electron-based analytical approaches.[5] Featured in **Figure 4A**, our research demonstrated the potential APT has in advancing the scientific understand of bone structure and interphases within mineralized tissues, which could provide insight to natural biomineralization processes on the atomic scale.

Figure 4. Atom probe tomography of mineralized tissues and osseointegrated interfaces.
(A) A 3D volume map shows the gradients of Ca distribution throughout human bone, where blue represents a lack of Ca and red represents high concentrations of Ca atoms. (B) A bright-field TEM micrograph and 3D APT atom map shows the likely presence of an inorganic interface between human bone and a retrieved dental implant. (C) A similar dental implant and human bone interface analyzed by a correlative combination of electron tomography, EELS tomography and APT highlights the integration of Ca atoms into the surface oxide of laser-modified titanium implants. Reproduced with permissions from [5,86,96].

APT has also been applied to osseointegrated materials and the interface between bone and biomaterials, for example mesoporous titania and rat bone[95] or human bone[96], and laser-modified titanium and human bone[86]. Sundell et al. used APT to investigate human bone-implant interfaces, where the resolving power of the technique provided insight into the rich calcium layer found at the bone-implant interface. [96] Meanwhile, we have further demonstrated the value of complimentary techniques, where we have evaluated a retrieved osseointegrated implant and characterized it using both on-axis electron tomography and APT, providing a holistic view on the functional connection between bone and titanium from both structural and chemical perspectives. [6] These two studies featured in **Figure 4B and C**, represent the first move towards a truly atomic scale chemical investigation of bone to implant interfaces.

Mechanical testing at the nanoscale:

The mechanical properties of mineralized tissues and interfaces have often been attributed to their whole bone hierarchical architecture.[97–100] Recent technological advances in mechanical testing and modeling methods have resulted in a trend towards nanoscale investigations of bone mechanical properties, both experimentally with atomic force microscopy (AFM)-nanoindentation[101,102], and by simulations with finite element modeling[73], molecular dynamics, or full atomistic models.[103,104] Some of these experimental approaches that probe nano level architectures of bone mineral or collagen fibrils, and incorporate image-based methods, are shown in **Figure 5**.
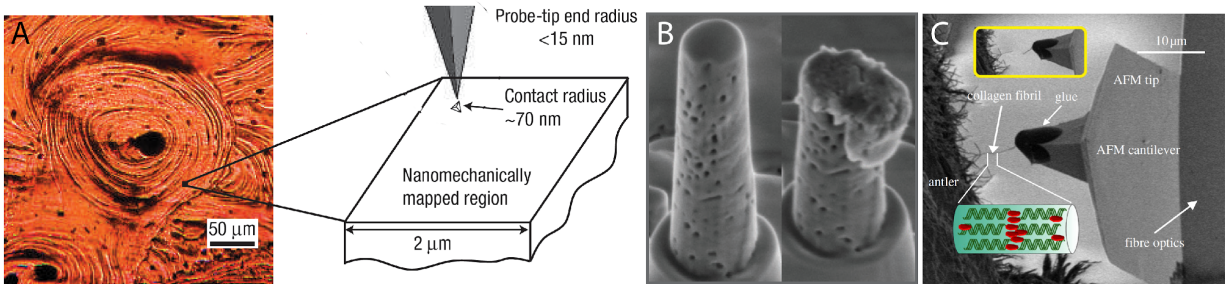
Figure 5. Imaging-based nanomechanical testing approaches for bone-like materials. (A) Optical microscopy image of an individual osteon and the AFM-based nanoindentation schematic used to infer energy dissipation through nanoscale structural heterogeneity, outlining the principal methods employed by Tai et al. (B) In another approach, nanopillars fabricated in FIB were placed under uniaxial compression to determine properties of distinct ordered/disordered zones within bone. (C) SEM image of the AFM configuration to evaluate the tensile properties of an individual antler collagen fiber with a combined AFM/SEM instrument. Reproduced with permissions from [101,107,109].

Firstly, experiments by Tai et al, exemplify the use of AFM for both imaging and nanomechanical strength determination of bone.[101] AFM, a high-resolution technique, uses a sharpened probe that either traces the surface at a defined height or mechanically interacts with the surface in contact mode. By probing the surface mechanically and measuring both the force exerted back onto the tip and the displacement, AFM-based nanoindentation can accurately determine nano-materials properties[105]. Using this approach, the stiffness of bone has been reported ranging between 2 to 30 GPa. This variable range is notable, as bone has natural interphases that could be related to increased calcium mineral and therefore increased stiffness.[101] AFM-based nanoindentation is therefore useful for probing local nano-scale properties in heterogeneous tissues.

Moreover, micro or nanopillars ranging in diameter from 250nm to 3000nm can be extracted from regions in bone using FIB for site-specific nano-compression testing.[106] Tertuliano et al. showed that pillars from distinct regions of bone structure (ordered, and disordered) performed

similarly under mechanical loading at both micro and nano length scales, which was possible through the use of a nanoindenter equipped with a flat plate. As noted in **Figure 5B**, experiments were completed until failure, and the fracture mechanism was then deduced to be brittle or shearing (not shown). [107] Interestingly, similar failure mechanisms and rates were observed among the various length scales investigated however, the authors postulated that the overall porosity of the extracellular matrix was the key determining factor for mechanical strength.[107]

At even smaller length scales, at the level of individual collagen fibrils, the role of mineralization on mechanical strength has been evaluated and modeled *in situ* using a micro-electromechanical device coupled to a confocal Raman microscope on synthetic collagen/apatite composites.[108] This work has shown the potential importance of degree of mineralization on strength of bone, where specimens with increased apatite composition showed higher elastic moduli, a mechanism suggested to be based on the molecular interlocking of collagen fibrils mediated by the mineral phase.[108]

Combined AFM and SEM imaging has also shed light on the effect of mineralization on mechanical properties of collagen fibrils in bone-like antler tissue, where similarly mineral content had a homogeneous effect on initial tensile strength. [109] These experiments used a more sophisticated approach, combing SEM and AFM, by which one single collagen fibril could be attached to the AFM probe and slowly pulled until fracture, **Figure 5C**. [109] Merging these two methods allowed the authors to perform an accurate investigation of single collagen fibrils, emphasizing the importance of developing unique characterization methods to solve biomaterials problems. Furthermore, atomistic calculations are also broadening the scope of mechanical

influences in bone structure towards the collagen fibril unit, where the role of mineral in strengthening bone has been further supported.[104]
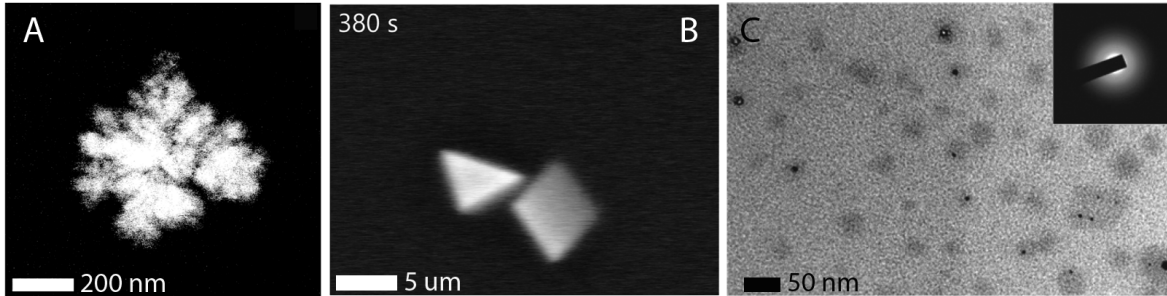
5. IN REAL-TIME

In situ mineralization:

The characterization of established biominerals and interfaces is of interest, but increasingly, there is a scientific desire to visualize the formation of tissues, or their mineral components in real-time, hydrated environments. Biomineral growth is well known to be templated by proteins such as collagen, and non-collagenous proteins in various biomineral systems[110], such as bone[111], periodontal tissues[112], and invertebrate systems[113,114]. Conventional observations of biomineralization processes have relied on halting mineralization at defined time points, either cryogenically or by chemical processes. Much progress has been made in understanding the role of collagen, non-collagenous proteins, and polyaspartic acid in the mineralization of collagen, in this way, presented in detail in other reviews and recent works.[115–117]

However, the dynamic processes of crystal growth are of interest to further understand the mechanisms behind biomineralization. Considerable progress has been made towards understanding the *in situ* growth of model systems, such as calcium carbonate for example, by an approach called liquid phase or *in situ* transmission electron microscopy.[118–121] This approach relies on the use of a specialized TEM holder that encapsulates liquid between electron-transparent silicon nitride or graphene membranes, enabling liquid to be safely placed within the vacuum of a TEM.[122] Several approaches to liquid cell TEM for the investigation of biominerals are available, including the simple encapsulation of liquid in static conditions, to the

flow of liquid via an inlet and outlet[123], or even mixing of different fluids within the TEM field of view.[124] This approach allows the real-time observation of mineral nanoparticle growth, and the interaction of relevant liquid systems or molecules on their growth mechanism. Optimization of experimental approaches to improve resolution, as well as the elucidation and elimination of electron beam-liquid interactions, and the development of approaches for quickly acquiring and processing data remain key challenges.[125,126]

Investigation into the role of proteins and inorganic additives has been a central theme for real-time *in situ* observations of biomineralization, a variety of which are highlighted in **Figure 6**. In these examples, the role of proteins or organic molecules on minerlization delay and resulting mineral assembly were investigated. Using a liquid flow TEM cell, the nacre-like calcium carbonate system was investigated to show that the intracrystalline C-RING protein AP7 delays the onset of nucleation and changes the spatial assembly of mineralized particles.[127] Other organic molecules such as poly(acrylic acid) (PAA) and poly(styrene sulfonate-co-maleic acid) (PSS-MA) have been shown to similarly contribute to the formation of a transient mineral phase, and ultimately morphologial changes in mineral formation of $CaCO_3$ as observed under atmospheric conditions in a unique inverted SEM instrument. [118] Polystyrene sulphonate (PSS) has also been shown to inhibit the nucleation of a transition phase of amorphous calcium carbonate during *in situ* TEM observations. [119] These observations provide insight into the role of mediating proteins and molecules during biomineralization and were only enabled by the encapsultated liquid cells or novel SEM assembly.

Figure 6. Real-time *in situ* biomineralization. (A) Liquid-phase scanning-TEM images show the formation of internal branching structures in $CaCO_3$ in the presence of AP7, a nacre C-RING protein. (B) An inverted atmospheric SEM allowed for observation of growth of $CaCO_3$ with triangular habit in the absence of any additives of under atmospheric conditions. (C) Amorphous Ca-PSS globules formed in liquid phase TEM with inset diffraction pattern confirming their amorphous structure. Reproduced with permissions from [118,119,127].

Moving towards more bone-like minerals systems, we have demonstrated the precipitation of hydroxyapatite-like calcium phosphates in static liquid cell TEM conditions.[128] This may provide insights into the morphological and crystal transitions that bone-like hydroxyapatite minerals undergo during bone formation. Further work to investigate the mineral phase interacting with its counterpart collagen through the real-time mineralization of collagen fibrils in solution is of key interest to the understanding of bone mineralization in healthy and pathological states. In addition, elucidating and reducing the role of the electron beam on the formation of biomineralized structures is highly relevant, as bone mineral content has been shown to be easily altered by repeated or high energy exposure to electron beams.[129]

Of course the experiments carried out in liquid cell TEM systems represent simplified *in vitro* models for *in vivo* mineralization. The other approach to mimicking an *in vivo* environment and mineralization is with relevant cell culture systems, which will not be discussed here, but is well covered in recent works and other reviews.[130–133]

Clinical evaluation of osseointegration:

Visualization of the mechanisms of bone growth and attachment in real-time on the nanoscale level, as described above, are simply not possible in clinical or *in vivo* models. In these scenarios, approaches to quantifying or qualifying osseointegration in patients rely on measures of mechanical implant stability, for example using quantitative ultrasound techniques[134], and lower resolution non-destructive imaging techniques, such a radiography[135], computed tomography (CT)[136], and magnetic resonance imaging (MRI).[137] Similar to high-resolution lab based imaging, clinical imaging has experienced a shift in emphasis from two-dimensional to three-dimensional imaging modalities, where technological advances in cone beam computed tomography (CBCT) are opening up a new realm of imaging possibilities for implant plannng and evaluation due to lower beam dose compared to conventional CT. However, review studies report inconsistencies in radiation dose values[138], and recommendations advise its sparing use, predominantly for surgical planning, and not as an evaluation tool.[139] Methods for assessing bone quality, independent of bone implants, are similarly varied between noninvasive imaging techniques and complementary *ex vivo* studies, which are well detailed elsewhere.[140]

6. CONCLUSIONS

Technological advancements across the fields of ion, electron, X-ray and atom probe microscopies are resulting in an increase in the use of multi-scale and multi-dimensional analyses for the investigation of bone interphases and biomaterials interfaces. A clear interest in moving towards multi-dimensional techniques that capture not only three-dimensional but

relevant chemical signatures is now emerging. Progress towards capturing real-time mineralization events using *in situ* liquid phase electron microscopy is another technological breakthrough, and paving the way for further mechanistic observations *in vitro*. With continuous developments in the imaging and characterization landscape, we expect our view of biomineralized tissues, such as bone, and the complexity of their interphases, including those to biomaterials, to continue to evolve.

REFERENCES

(1)   Bonewald, L. F. Mechanosensation and Transduction in Osteocytes. *Bonekey Osteovision* **2006**, *3* (10), 7–15.

(2)   Weiner, S.; Traub, W. Bone structure: from angstroms to microns. *FASEB J.* **1992**, *6* (3), 879–885.

(3)   Grandfield, K. Bone, implants, and their interfaces. *Phys. Today* **2015**, *68* (4), 40–45.

(4)   Ho, S. P.; Balooch, M.; Marshall, S. J.; Marshall, G. W. Local properties of a functionally graded interphase between cementum and dentin. *J. Biomed. Mater. Res.* **2004**, *70A* (3), 480–489.

(5)   Langelier, B.; Wang, X.; Grandfield, K. Atomic scale chemical tomography of human bone. *Sci. Rep.* **2017**.

(6)   Wang, X.; Shah, F. A.; Palmquist, A.; Grandfield, K. 3D Characterization of Human Nano-osseointegration by On-Axis Electron Tomography without the Missing Wedge. *ACS Biomater. Sci. Eng.* **2017**, *3* (1), 49–55.

(7)   Brown, W. E.; Chow, L. C. Chemical Properties of Bone Mineral. *Annu. Rev. Mater. Sci.* **1976**, *6* (1), 213–236.

(8)   Wegst, U. G. K.; Bai, H.; Saiz, E.; Tomsia, A. P.; Ritchie, R. O. Bioinspired structural materials. *Nat. Mater.* **2014**, *14* (1), 23–36.

(9)   Ritchie, R. O.; Buehler, M. J.; Hansma, P. Plasticity and toughness in bone. *Phys. Today* **2009**, *62*, 41.

(10)   Reznikov, N.; Shahar, R.; Weiner, S. Bone hierarchical structure in three dimensions. *Acta Biomater.* **2014**, *10* (9), 3815–3826.

(11) Li, H.; Ghazanfari, R.; Zacharaki, D.; Lim, H. C.; Scheding, S. Isolation and characterization of primary bone marrow mesenchymal stromal cells. *Ann. N. Y. Acad. Sci.* **2016**, *1370* (1), 109–118.

(12) Florencio-Silva, R.; Rodrigues, G.; Sasso, S.; Sasso-Cerri, E.; Simões, M. J.; Cerri, P. S. Biology of Bone Tissue: Structure, Function, and Factors That Influence Bone Cells. *Biomed Res. Int.* **2015**, *2015*, 1–17.

(13) Hadjidakis, D. J.; Androulakis, I. I. Bone remodeling. *Ann. N. Y. Acad. Sci.* **2006**, *1092*, 385–396.

(14) Reznikov, N.; Chase, H.; Brumfeld, V.; Shahar, R.; Weiner, S. The 3D structure of the collagen fibril network in human trabecular bone: Relation to trabecular organization. *Bone* **2015**, *71*, 189–195.

(15) Brånemark, P. I. Osseointegration and its experimental background. *J. Prosthet. Dent.* **1983**, *50* (3), 399–410.

(16) Saini, M.; Singh, Y.; Arora, P.; Arora, V.; Jain, K. Implant biomaterials: A comprehensive review. *World J. Clin. cases* **2015**, *3* (1), 52–57.

(17) Long, M.; Rack, H. . Titanium alloys in total joint replacement?a materials science perspective. *Biomaterials* **1998**, *19* (18), 1621–1639.

(18) Palmquist, A.; Grandfield, K.; Norlindh, B. Bone-titanium oxide interface in humans revealed by transmission electron microscopy and electron tomography. *J. R. Soc. Interface* **2012**, *9* (67), 396–400.

(19) Roberts, T. T.; Rosenbaum, A. J. Bone grafts, bone substitutes and orthobiologics: the bridge between basic science and clinical advancements in fracture healing. *Organogenesis* **2012**, *8* (4).

(20)   Sterling, J. A.; Guelcher, S. A. Biomaterial scaffolds for treating osteoporotic bone. *Curr. Osteoporos. Rep.* **2014**, *12* (1), 48–54.

(21)   McKee, M. D.; Pedraza, C. E.; Kaartinen, M. T. Osteopontin and Wound Healing in Bone. *Cells Tissues Organs* **2011**, *194* (2–4).

(22)   Teo, A. J. T.; Mishra, A.; Park, I.; Kim, Y.-J.; Park, W.-T.; Yoon, Y.-J. Polymeric Biomaterials for Medical Implants and Devices. *ACS Biomater. Sci. Eng.* **2016**, *2* (4), 454–472.

(23)   Niinomi, M.; Nakai, M. Titanium-Based Biomaterials for Preventing Stress Shielding between Implant Devices and Bone. *Int. J. Biomater.* **2011**, *2011*, 1-10.

(24)   Lindahl, H. Epidemiology of periprosthetic femur fracture around a total hip arthroplasty. *Injury* **2007**, *38* (6), 651–654.

(25)   Bordier, P. J.; Chot, S. T. Quantitative histology of metabolic bone disease. *Clin. Endocrinol. Metab.* **1972**, *1* (1), 197–215.

(26)   Bobyn, J. D.; Pillar, R. M.; Cameron, H. U.; Weatherly, G. C. The Optimum Pore Size for the Fixation of Porous-Surfaced Metal Implants by the Ingrowth of Bone. *Clin. Orthop. Relat. Res.* **1980**, *150*, 263–270.

(27)   Roschger, P.; Fratzl, P.; Eschberger, J.; Klaushofer, K. Validation of quantitative backscattered electron imaging for the measurement of mineral density distribution in human bone biopsies. *Bone* **1998**, *23* (4), 319–326.

(28)   Roschger, P.; Misof, B.; Paschalis, E.; Fratzl, P.; Klaushofer, K. Changes in the Degree of Mineralization with Osteoporosis and its Treatment. *Curr. Osteoporos. Rep.* **2014**, *12* (3), 338–350.F

(29)   Harrington, J.; Holmyard, D.; Silverman, E.; Sochett, E.; Grynpas, M. Bone

histomorphometric changes in children with rheumatic disorders on chronic glucocorticoids. *Pediatric Rheumatology Online J.* **2016**, 14 (1), 50 -58.

(30) Boerckel, J. D.; Mason, D. E.; McDermott, A. M. Microcomputed tomography: approaches and applications in bioengineering. *Stem Cell Res. Ther.* **2014**, *5* (6), 144.

(31) Georgiadis, M.; Müller, R.; Schneider, P. Techniques to assess bone ultrastructure organization: orientation and arrangement of mineralized collagen fibrils. *J. R. Soc. Interface* **2016**, *13* (119).

(32) Granke, M.; Gourrier, A.; Rupin, F.; Raum, K.; Peyrin, F.; Burghammer, M.; Saïed, A.; Laugier, P. Microfibril Orientation Dominates the Microelastic Properties of Human Bone Tissue at the Lamellar Length Scale. *PLoS One* **2013**, *8* (3), e58043.

(33) Bertoldi, S.; Farè, S.; Tanzi, M. C. Assessment of scaffold porosity: the new route of micro-CT. *J. Appl. Biomater. Biomech.* **2011**, *9* (3), 165–175.

(34) Thorfve, A.; Palmquist, A.; Grandfield, K. Three-dimensional analytical techniques for evaluation of osseointegrated titanium implants. *Mater. Sci. Technol.* **2015**, *31* (2), 174–179.

(35) Otsuki, B.; Takemoto, M.; Fujibayashi, S.; Neo, M.; Kokubo, T.; Nakamura, T. Pore throat size and connectivity determine bone and tissue ingrowth into porous implants: Three-dimensional micro-CT based structural analyses of porous bioactive titanium implants. *Biomaterials* **2006**, *27* (35), 5892–5900.

(36) Varga, P.; Pacureanu, A.; Langer, M.; Suhonen, H.; Hesse, B.; Grimal, Q.; Cloetens, P.; Raum, K.; Peyrin, F. Investigation of the three-dimensional orientation of mineralized collagen fibrils in human lamellar bone using synchrotron X-ray phase nano-tomography. *Acta Biomater.* **2013**, *9* (9), 8118–8127.

(37)   Mobus, G.; Inkson, B. J. Nanoscale tomography in materials science. *Mater. Today* **2007**, *10* (12), 18–25.

(38)   Giannuzzi, L.; Geurts, R.; Ringnalda, J. 2 keV Ga+ FIB Milling for Reducing Amorphous Damage in Silicon. *Microsc. Microanal.* **2005**, *11* (S02), 828–829.

(39)   Narayan, K.; Subramaniam, S. Focused ion beams in biology. *Nat. Methods* **2015**, *12* (11), 1021–1031.

(40)   Grandfield, K.; Engqvist, H. Focused Ion Beam in the Study of Biomaterials and Biological Matter. *Adv. Mater. Sci. Eng.* **2012**, *2012*, 1–6 DOI: 10.1155/2012/841961.

(41)   Giannuzzi, L.; Phifer, D.; Giannuzzi, N.; Capuano, M. Two-Dimensional and 3-Dimensional Analysis of Bone/Dental Implant Interfaces With the Use of Focused Ion Beam and Electron Microscopy. *J. Oral Maxillofac. Surg.* **2007**, *65* (4), 737–747.

(42)   Schneider, P.; Meier, M.; Wepf, R.; Müller, R. Serial FIB/SEM imaging for quantitative 3D assessment of the osteocyte lacuno-canalicular network. *Bone* **2011**, *49* (2), 304–311.

(43)   Reznikov, N.; Almany-Magal, R.; Shahar, R.; Weiner, S. Three-dimensional imaging of collagen fibril organization in rat circumferential lamellar bone using a dual beam electron microscope reveals ordered and disordered sub-lamellar structures. *Bone* **2013**, *52* (2), 676–683.

(44)   Reznikov, N.; Shahar, R.; Weiner, S. Three-dimensional structure of human lamellar bone: the presence of two different materials and new insights into the hierarchical organization. *Bone* **2014**, *59*, 93–104.

(45)   Rucci, N. Molecular biology of bone remodelling. *Clin. Cases Miner. Bone Metab.* **2008**, *5* (1), 49–56.

(46)   Dallas, S. L.; Bonewald, L. F. Dynamics of the transition from osteoblast to osteocyte.

Ann. N. Y. Acad. Sci. **2010**, *1192*, 437–443.

(47) Shah, F. A.; Zanghellini, E.; Matic, A.; Thomsen, P.; Palmquist, A. The Orientation of Nanoscale Apatite Platelets in Relation to Osteoblastic–Osteocyte Lacunae on Trabecular Bone Surface. *Calcif. Tissue Int.* **2016**, *98* (2), 193–205.

(48) Steflik, D. E.; Sisk, A. L.; Parr, G. R.; Lake, F. T.; Hanes, P. J.; Berkery, D. J.; Brewer, P. Transmission electron and high-voltage electron microscopy of osetocyte cellular processes extending to the dental implant surface. *J. Biomed. Mater. Res. Part B Appl. Biomater.* **1994**, *28* (9), 1095–1107.

(49) Shah, F. A.; Wang, X.; Thomsen, P.; Grandfield, K.; Palmquist, A. High-Resolution Visualization of the Osteocyte Lacuno-Canalicular Network Juxtaposed to the Surface of Nanotextured Titanium Implants in Human. *ACS Biomater. Sci. Eng.* **2015**, *1* (5), 305–313.

(50) Shah, F. A.; Snis, A.; Matic, A.; Thomsen, P.; Palmquist, A. 3D printed Ti6Al4V implant surface promotes bone maturation and retains a higher density of less aged osteocytes at the bone-implant interface. *Acta Biomater.* **2016**, *30*, 357–367.

(51) Pacureanu, A.; Larrue, A.; Langer, M.; Olivier, C.; Muller, C.; Lafage-Proust, M. H.; Peyrin, F. Adaptive filtering for enhancement of the osteocyte cell network in 3D microtomography images. *IRBM* **2013**, *34* (1), 48–52.

(52) Schneider, P.; Meier, M.; Wepf, R.; Müller, R. Towards quantitative 3D imaging of the osteocyte lacuno-canalicular network. *Bone* **2010**, *47* (5), 848–858.

(53) Schaff, F.; Bech, M.; Zaslansky, P.; Jud, C.; Liebi, M.; Guizar-Sicairos, M.; Pfeiffer, F. Six-dimensional real and reciprocal space small-angle X-ray scattering tomography. *Nature* **2015**, *527* (7578), 353–356.

(54) Kerschnitzki, M.; Kollmannsberger, P.; Burghammer, M.; Duda, G. N.; Weinkamer, R.; Wagermaier, W.; Fratzl, P. Architecture of the osteocyte network correlates with bone material quality. *J. Bone Miner. Res.* **2013**, *28* (8), 1837–1845.

(55) Steflik, D. E.; Corpe, R. S.; Lake, F. T.; Young, T. R.; Sisk, A. L.; Parr, G. R.; Hanes, P. J.; Berkery, D. J. Ultrastructural analyses of the attachment (bonding) zone between bone and implanted biomaterials. *J. Biomed. Mater. Res. Part A* **1998**, *39* (4), 611–620.

(56) Neo, M.; Kotani, S.; Nakamura, T.; Yamamuro, T.; Ohtsuki, C.; Kokubo, T.; Bando, Y. A comparative study of ultrastructures of the interfaces between four kinds of surface-active ceramic and bone. *J. Biomed. Mater. Res.* **1992**, *26* (11), 1419–1432.

(57) de Bruijn, J. D.; van Blitterswijk, C. A.; Davies, J. E. Initial bone matrix formation at the hydroxyapatite interface in vivo. *J. Biomed. Mater. Res.* **1995**, *29* (1), 89–99.

(58) Hemmerlé, J.; Önçag, A.; Ertürk, S. Ultrastructural features of the bone response to a plasma-sprayed hydroxyapatite coating in sheep. *J. Biomed. Mater. Res.* **1997**, *36* (3), 418–425.

(59) McNally, E.; Nan, F.; Botton, G. A.; Schwarcz, H. P. Scanning transmission electron microscopic tomography of cortical bone using Z-contrast imaging. *Micron* **2013**, *49*, 46–53.

(60) Jantou, V.; Turmaine, M.; West, G. D.; Horton, M. A.; McComb, D. W. Focused ion beam milling and ultramicrotomy of mineralised ivory dentine for analytical transmission electron microscopy. *Micron* **2009**, *40* (4), 495–501.

(61) Volkert, C. A.; Busch, S.; Heiland, B.; Dehm, G. Transmission electron microscopy of fluorapatite-gelatine composite particles prepared using focused ion beam milling. *J. Microsc.* **2004**, *214* (3), 208–212.

(62) Coutinho, E.; Jarmar, T.; Svahn, F.; Neves, A. A.; Verlinden, B.; van Meerbeek, B.; Engqvist, H. Ultrastructural characterization of tooth-biomaterial interfaces prepared with broad and focused ion beams. *Dent. Mater.* **2009**, *25* (11), 1325–1337.

(63) Engqvist, H.; Svahn, F.; Jarmar, T.; Detsch, R.; Mayr, H.; Thomsen, P.; Ziegler, G. A novel method for producing electron transparent films of interfaces between cells and biomaterials. *J. Mater. Sci. Mater. Med.* **2007**, *19* (1), 467–470.

(64) Jarmar, T.; Palmquist, A.; Brånemark, R.; Hermansson, L.; Engqvist, H.; Thomsen, P. Technique for preparation and characterization in cross-section of oral titanium implant surfaces using focused ion beam and transmission electron microscopy. *J. Biomed. Mater. Res. Part A* **2008**, *87A* (4), 1003–1009.

(65) Grandfield, K.; McNally, E. A.; Palmquist, A.; Botton, G. A.; Thomsen, P.; Engqvist, H. Visualizing biointerfaces in three dimensions: electron tomography of the bone-hydroxyapatite interface. *J. R. Soc. Interface* **2010**, *7* (51), 1497–1501.

(66) McNally, E. A.; Schwarcz, H. P.; Botton, G. A.; Arsenault, A. L. A model for the ultrastructure of bone based on electron microscopy of ion-milled sections. *PLoS One* **2012**, *7* (1), 1–12.

(67) Rubino, S.; Melin, P.; Spellward, P.; Leifer, K. Cryo-electron microscopy specimen preparation by means of a focused ion beam. *J. Vis. Exp.* **2014**, No. 89, e51463–e51463.

(68) Schwarcz, H. P. The ultrastructure of bone as revealed in electron microscopy of ion-milled sections. *Semin. Cell Dev. Biol.* **2015**, *46*, 44–50.

(69) Alexander, B.; Daulton, T. L.; Genin, G. M.; Lipner, J.; Pasteris, J. D.; Wopenka, B.; Thomopoulos, S. The nanometre-scale physiology of bone: steric modelling and scanning transmission electron microscopy of collagen–mineral structure. *J. R. Soc. Interface* **2012**,

9 (73).

(70)   Weiner, S.; Traub, W. Organization of hydroxyapatite crystals within collagen fibrils. *FEBS Lett.* **1986**, *206* (2), 262–266.

(71)   Weiner, S.; Traub, W. Bone structure: from angstroms to microns. *FASEB J.* **1992**, *6* (3), 879–885.

(72)   Schwarcz, H. P.; Abueidda, D.; Jasiuk, I. The Ultrastructure of Bone and Its Relevance to Mechanical Properties. *Front. Phys.* **2017**.

(73)   Abueidda, D. W.; Sabet, F. A.; Jasiuk, I. M. Modeling of Stiffness and Strength of Bone at Nanoscale. *J. Biomech. Eng.* **2017**.

(74)   Midgley, P. A.; Weyland, M. 3D electron microscopy in the physical sciences: the development of Z-contrast and EFTEM tomography. *Ultramicroscopy* **2003**, *96* (3–4), 413–431.

(75)   Midgley, P. A.; Dunin-Borkowski, R. E. Electron tomography and holography in materials science. *Nat. Mater.* **2009**, *8* (4), 271–280.

(76)   Ercius, P.; Alaidi, O.; Rames, M. J.; Ren, G. Electron Tomography: A Three-Dimensional Analytic Tool for Hard and Soft Materials Research. *Advanced Materials*. 2015.

(77)   Grandfield, K.; Palmquist, a.; Engqvist, H. High-resolution three-dimensional probes of biomaterials and their interfaces. *Philos. Trans. R. Soc. A Math. Phys. Eng. Sci.* **2012**, *370*, 1337–1351.

(78)   Miao, J.; Ercius, P.; Billinge, S. J. L. Atomic electron tomography: 3D structures without crystals. *Science* **2016**, *353* (6306), aaf2157.

(79)   Landis, W. J.; Hodgens, K. J.; Arena, J.; Song, M. J.; McEwen, B. F. Structural relations between collagen and mineral in bone as determined by high voltage electron microscopic

tomography. *Microsc. Res. Tech.* **1996**, *33* (2), 192–202.

(80)   Landis, W. J.; Song, M. J.; Leith, A.; McEwen, L.; McEwen, B. F. Mineral and Organic Matrix Interaction in Normally Calcifying Tendon Visualized in Three Dimensions by High-Voltage Electron Microscopic Tomography and Graphic Image Reconstruction. *J. Struct. Biol.* **1993**, *110* (1), 39–54.

(81)   Landis, W. J.; Hodgens, K. J.; Song, M. J.; Arena, J.; Kiyonaga, S.; Marko, M.; Owen, C.; McEwen, B. F. Mineralization of Collagen May Occur on Fibril Surfaces: Evidence from Conventional and High-Voltage Electron Microscopy and Three-Dimensional Imaging. *J. Struct. Biol.* **1996**, *117* (1), 24–35.

(82)   McNally, E.; Nan, F.; Botton, G. a; Schwarcz, H. P. Scanning transmission electron microscopic tomography of cortical bone using Z-contrast imaging. *Micron* **2013**, *49*, 46–53.

(83)   Grandfield, K.; Palmquist, A.; Engqvist, H. Three-dimensional structure of laser-modified Ti6Al4V and bone interface revealed with STEM tomography. *Ultramicroscopy* **2013**, *127*, 48–52.

(84)   Grandfield, K.; Engqvist, H. Characterization of dental interfaces with electron tomography. *Biointerphases* **2014**, *9* (2), 29001.

(85)   Bals, S.; Goris, B.; Liz-Marzán, L. M.; Van Tendeloo, G. Three-Dimensional Characterization of Noble-Metal Nanoparticles and their Assemblies by Electron Tomography. *Angew. Chemie Int. Ed.* **2014**, *53* (40), 10600–10610.

(86)   Wang, X.; Langelier, B.; Palmquist, A.; Grandfield, K. Biomineralization at Interfaces Revealed with 4D Electron and Atom Probe Tomographies. *Microsc. Microanal.* **2015**, *21* (S3).

(87)   Kelly, T. F.; Miller, M. K. Atom probe tomography. *Rev. Sci. Instrum.* **2007**, *78* (3), 31101.

(88)   Narayan, K.; Prosa, T. J.; Fu, J.; Kelly, T. F.; Subramaniam, S. Chemical mapping of mammalian cells by atom probe tomography. *J. Struct. Biol.* **2012**, *178* (2), 98–107.

(89)   Perea, D. E.; Liu, J.; Bartrand, J.; Dicken, Q.; Thevuthasan, S. T.; Browning, N. D.; Evans, J. E. Atom Probe Tomographic Mapping Directly Reveals the Atomic Distribution of Phosphorus in Resin Embedded Ferritin. *Sci. Rep.* **2016**, *6* (1), 22321.

(90)   Gordon, L. M.; Joester, D. Nanoscale chemical tomography of buried organic-inorganic interfaces in the chiton tooth. *Nature* **2011**, *469* (7329), 194–197.

(91)   Gordon, L. M.; Tran, L.; Joester, D. Atom Probe Tomography of Apatites and Bone-Type Mineralized Tissues. *ACS Nano* **2012**, *6* (12), 10667–10675.

(92)   La Fontaine, A.; Zavgorodniy, A.; Liu, H.; Zheng, R.; Swain, M.; Cairney, J. Atomic-scale compositional mapping reveals Mg-rich amorphous calcium phosphate in human dental enamel. *Sci. Adv.* **2016**, *2* (9), e1601145–e1601145.

(93)   Gordon, L. M.; Cohen, M. J.; MacRenaris, K. W.; Pasteris, J. D.; Seda, T.; Joester, D. Dental materials. Amorphous intergranular phases control the properties of rodent tooth enamel. *Science (80-.).* **2015**, *347* (6223), 746–750.

(94)   Gordon, L. M.; Joester, D. Mapping residual organics and carbonate at grain boundaries and the amorphous interphase in mouse incisor enamel. *Front. Physiol.* **2015**, *6*, 57.

(95)   Karlsson, J.; Sundell, G.; Thuvander, M.; Andersson, M. Atomically resolved tissue integration. *Nano Lett.* **2014**, *14* (8), 4220–4223.

(96)   Sundell, G.; Dahlin, C.; Andersson, M.; Thuvander, M. The bone-implant interface of dental implants in humans on the atomic scale. *Acta Biomater.* **2017**, *48*, 445–450.

(97)   Ritchie, R. O.; Buehler, M. J.; Hansma, P. Plasticity and toughness in bone. *Phys. Today*

2009, *62* (6), 41–47.

(98)   Zimmermann, E. A.; Ritchie, R. O. Bone as a Structural Material. *Adv. Healthc. Mater.* **2015**, *4* (9), 1287–1304.

(99)   Zimmermann, E. A.; Busse, B.; Ritchie, R. O. The fracture mechanics of human bone: influence of disease and treatment. *Bonekey Rep.* **2015**, *4*, 743.

(100)   Zimmermann, E. A.; Barth, H. D.; Ritchie, R. O. The Multiscale Origins of Fracture Resistance in Human Bone and Its Biological Degradation. *Jom* **2012**, *64* (4), 486–493.

(101)   Tai, K.; Dao, M.; Suresh, S.; Palazoglu, A.; Ortiz, C. Nanoscale heterogeneity promotes energy dissipation in bone. *Nat. Mater.* **2007**, *6* (6), 454–462.

(102)   Rodriguez-Florez, N.; Oyen, M. L.; Shefelbine, S. J. Insight into differences in nanoindentation properties of bone. *J. Mech. Behav. Biomed. Mater.* **2013**, *18*, 90–99.

(103)   Depalle, B.; Qin, Z.; Shefelbine, S. J.; Buehler, M. J. Large Deformation Mechanisms, Plasticity, and Failure of an Individual Collagen Fibril With Different Mineral Content. *J. Bone Miner. Res.* **2016**, *31* (2), 380–390.

(104)   Nair, A. K.; Gautieri, A.; Chang, S.-W.; Buehler, M. J. Molecular mechanics of mineralized collagen fibrils in bone. *Nat. Commun.* **2013**, *4*, 1724.

(105)   Jalili, N.; Lazminarayana, K. A review of atomic force microscopy imaging systems: application to molecular metrology and biological sciences. *Mechatronics* **2004**, *14* (8), 907–945.

(106)   Schwiedrzik, J.; Raghavan, R.; Bürki, A.; LeNader, V.; Wolfram, U.; Michler, J.; Zysset, P. In situ micropillar compression reveals superior strength and ductility but an absence of damage in lamellar bone. *Nat. Mater.* **2014**, *13* (7), 740–747.

(107)   Tertuliano, O. A.; Greer, J. R. The nanocomposite nature of bone drives its strength and

damage resistance. *Nat. Mater.* **2016**, 15, 1195-1202.

(108) Chatzipanagis, K.; Baumann, C. G.; Sandri, M.; Sprio, S.; Tampieri, A.; Kröger, R. In situ mechanical and molecular investigations of collagen/apatite biomimetic composites combining Raman spectroscopy and stress-strain analysis. *Acta Biomater.* **2016**, *46* (C), 278–285.

(109) Hang, F.; Barber, A. H. Nano-mechanical properties of individual mineralized collagen fibrils from bone tissue. *J. R. Soc. Interface* **2011**, *8* (57), 500–505.

(110) Addadi, L.; Gal, A.; Faivre, D.; Scheffel, A.; Weiner, S. Control of Biogenic Nanocrystal Formation in Biomineralization. *Isr. J. Chem.* **2016**, *56* (4), 227–241.

(111) Wang, Y.; Azaïs, T.; Robin, M.; Vallée, A.; Catania, C.; Legriel, P.; Pehau-Arnaudet, G.; Babonneau, F.; Giraud-Guille, M.-M.; Nassif, N. The predominant role of collagen in the nucleation, growth, structure and orientation of bone apatite. *Nat. Mater.* **2012**, *11* (8), 724–733.

(112) Lausch, A. J.; Quan, B. D.; Miklas, J. W.; Sone, E. D. Extracellular Matrix Control of Collagen Mineralization In Vitro. *Adv. Funct. Mater.* **2013**, *23* (39), 4906–4912.

(113) Evans, J. S. "Tuning in" to Mollusk Shell Nacre- and Prismatic-Associated Protein Terminal Sequences. Implications for Biomineralization and the Construction of High Performance Inorganic−Organic Composites. *Chem. Rev.* **2008**, *108* (11), 4455–4462.

(114) Bahn, S. Y.; Jo, B. H.; Hwang, B. H.; Choi, Y. S.; Cha, H. J. Role of Pif97 in Nacre Biomineralization: In Vitro Characterization of Recombinant Pif97 as a Framework Protein for the Association of Organic–Inorganic Layers in Nacre. *Cryst. Growth Des.* **2015**, *15* (8), 3666–3673.

(115) Nudelman, F.; Lausch, A. J.; Sommerdijk, N. A. J. M.; Sone, E. D. In vitro models of

collagen biomineralization. *J. Struct. Biol.* **2013**, *183* (2), 258–269.

(116) Jiao, K.; Niu, L. N.; Ma, C. F.; Huang, X. Q.; Pei, D. D.; Luo, T.; Huang, Q.; Chen, J. H.; Tay, F. R. Complementarity and Uncertainty in Intrafibrillar Mineralization of Collagen. *Adv. Funct. Mater.* **2016**, *26* (38), 6858–6875.

(117) Lausch, A. J.; Quan, B. D.; Miklas, J. W.; Sone, E. D. Extracellular Matrix Control of Collagen Mineralization In Vitro. *Adv. Funct. Mater.* **2013**, *23* (39), 4906–4912.

(118) Verch, A.; Morrison, I. E. G.; Locht, R. van de; Kröger, R. In situ electron microscopy studies of calcium carbonate precipitation from aqueous solution with and without organic additives. *J. Struct. Biol.* **2013**, *183* (2), 270–277.

(119) Smeets, P. J. M.; Cho, K. R.; Kempen, R. G. E.; Sommerdijk, N. A. J. M.; De Yoreo, J. J. Calcium carbonate nucleation driven by ion binding in a biomimetic matrix revealed by in situ electron microscopy. *Nat. Mater.* **2015**, *14* (4), 394–399.

(120) De Yoreo, J. J.; Gilbert, P. U. P. A.; Sommerdijk, N. A. J. M.; Penn, R. L.; Whitelam, S.; Joester, D.; Zhang, H.; Rimer, J. D.; Navrotsky, A.; Banfield, J. F.; et al. Crystallization by particle attachment in synthetic, biogenic, and geologic environments. *Science (80-.).* **2015**, *349* (6247), aaa6760-aaa6760.

(121) Nielsen, M. H.; Aloni, S.; De Yoreo, J. J. In situ TEM imaging of $CaCO_3$ nucleation reveals coexistence of direct and indirect pathways. *Science (80-.).* **2014**, *345* (6201), 1158–1162.

(122) *Liquid Cell Electron Microscopy*; Ross, F. M., Ed.; Cambridge University Press: Cambridge, 2017.

(123) Klein, K. L.; Anderson I. M.; De Jonge, N. Transmission electron microscopy with a liquid flow cell. *J. Microsc.* **2011**, *242* (2), 117–123

(124) Nielsen, M. H.; Yoreo, J. J. De. Liquid Cell TEM for Studying Environmental and Biological Mineral Systems. In *Liquid Cell Electron Microscopy*; Ross, F. M., Ed.; Cambridge University Press: Cambridge; pp 316–333.

(125) Liao, H.-G.; Zheng, H. Liquid Cell Transmission Electron Microscopy. *Annu. Rev. Phys. Chem.* **2016**, *67* (1), 719–747 DOI: 10.1146/annurev-physchem-040215-112501.

(126) Ross, F. M. Opportunities and challenges in liquid cell electron microscopy. *Science* **2015**, *350* (6267), aaa9886.

(127) Perovic, I.; Verch, A.; Chang, E. P.; Rao, A.; Cölfen, H.; Kröger, R.; Evans, J. S. An oligomeric C-RING nacre protein influences prenucleation events and organizes mineral nanoparticles. *Biochemistry* **2014**, *53* (46), 7259–7268.

(128) Wang, X.; Yang, J.; Andrei, C.; Soleymani, L.; Grandfield, K. Biomineralization of Hydroxyapatite Revealed by in situ Electron Microscopy. *Microsc. Microanal.* **2016**, *22* (S3), 746–747.

(129) Bloebaum, R. D.; Holmes, J. L.; Skedros, J. G. Mineral content changes in bone associated with damage induced by the electron beam. *Scanning* **2005**, *27* (5), 240–248.

(130) Boskey, A. L.; Roy, R. Cell culture systems for studies of bone and tooth mineralization. *Chem. Rev.* **2008**, *108* (11), 4716–4733.

(131) Boskey, A. L.; Stiner, D.; Doty, S. B.; Binderman, I.; Leboy, P. Studies of mineralization in tissue culture: optimal conditions for cartilage calcification. *Bone Miner.* **1992**, *16* (1), 11–36.

(132) Hoemann, C. D.; El-Gabalawy, H.; McKee, M. D. In vitro osteogenesis assays: influence of the primary cell source on alkaline phosphatase activity and mineralization. *Pathol. Biol.* **2009**, *57* (4), 318–323.

(133) Pujari-Palmer, M.; Pujari-Palmer, S.; Lu, X.; Lind, T.; Melhus, H. kan; Engstrand, T.; Karlsson Ott, M.; Engqvist, H. Pyrophosphate Stimulates Differentiation, Matrix Gene Expression and Alkaline Phosphatase Activity in Osteoblasts. *PLoS One* **2016**, *11* (10), e0163530-13.

(134) Mathieu, V.; Vayron, R.; Richard, G.; Lambert, G.; Naili, S.; Meningaud, J.-P.; Haiat, G. Biomechanical determinants of the stability of dental implants: Influence of the bone–implant interface properties. *J. Biomech.* **2013**, *47*, 3–13.

(135) Monsour, P.; Dudhia, R. Implant radiography and radiology. *Aust. Dent. J.* **2008**, *53* (1), 11–25.

(136) Gupta, S.; Patil, N.; Solanki, J.; Singh, R.; Laller, S. Oral Implant Imaging: A Review. *Malays. J. Med. Sci.* **2015**, *22* (3), 7–17.

(137) Korn, P.; Elschner, C.; Schulz, M. C.; Range, U.; Mai, R.; Scheler, U. MRI and dental implantology: Two which do not exclude each other. *Biomaterials* **2015**, *53*, 634–645.

(138) De Vos, W.; Casselman, J.; Swennen, G. R. J. Cone-beam computerized tomography (CBCT) imaging of the oral and maxillofacial region: A systematic review of the literature. *Int. J. Oral Maxillofac. Surg.* **2009**, *38* (6), 609–625.

(139) Benavides, E.; Rios, H. F.; Ganz, S. D.; An, C.-H.; Resnik, R.; Reardon, G. T.; Feldman, S. J.; Mah, J. K.; Hatcher, D.; Kim, M.-J.; et al. Use of Cone Beam Computed Tomography in Implant Dentistry. *Implant Dent.* **2012**, *21* (2), 78–86.

(140) Donnelly, E. Methods for assessing bone quality: a review. *Clin. Orthop. Relat. Res.* **2011**, *469* (8), 2128–2138.

(141) Schwarcz, H. P.; McNally, E. A.; Botton, G. A. Dark-field transmission electron microscopy of cortical bone reveals details of extrafibrillar crystals. *J. Struct. Biol.* **2014**,

188 (3), 240–248.

For Table of Contents Use Only

Multi-Scale Imaging of Biomaterials
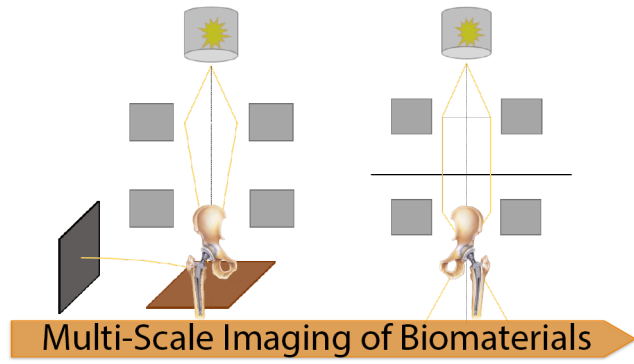
Manuscript Title: Advances in Multi-Scale Characterization Techniques of Bone and Biomaterials Interfaces

Authors: Dakota M. Binkley and K. Grandfield